

What causes the ultraviolet extinction bump at the cosmic dawn?

Qi Li^{1,2}, X.J. Yang^{1,2*}, and Aigen Li^{2†}

¹Hunan Key Laboratory for Stellar and Interstellar Physics and School of Physics and Optoelectronics, Xiangtan University, Hunan 411105, China

²Department of Physics and Astronomy, University of Missouri, Columbia, MO 65211, USA

ABSTRACT

The enigmatic ultraviolet (UV) extinction bump at 2175 Å, the strongest spectroscopic absorption feature superimposed on the interstellar extinction curve, has recently been detected at the cosmic dawn by the James Webb Space Telescope (JWST) in JADES-GS-z6-0, a distant galaxy at redshift $z \approx 6.71$, corresponding to a cosmic age of just 800 million years after the Big Bang. Although small graphite grains have historically long been suggested as the carrier of the 2175 Å extinction bump and graphite grains are expected to have already been pervasive in the early Universe, in this work we demonstrate that small graphite grains are not responsible for the UV extinction bump seen at the cosmic dawn in JADES-GS-z6-0, as the extinction bump arising from small graphite grains is too broad and peaks at wavelengths that are too short to be consistent with what is seen in JADES-GS-z6-0.

Key words: ISM: dust, extinction — ISM: lines and bands — ISM: molecules

1 INTRODUCTION

Due to its unprecedentedly high sensitivity, the *James Webb Space Telescope* (JWST) is capable of detecting rest-frame ultraviolet (UV) emission from very high-redshift galaxies, and therefore provides a paradigm-shifting view of early galaxy evolution. The rest-frame UV starlight emission is absorbed and scattered by solid dust grains in the galaxy’s interstellar medium (ISM). The wavelength dependence of the dust absorption and scattering—their combination is called extinction—exhibits a strong spectral band peaking at ~ 2175 Å. As the most prominent spectroscopic feature in the interstellar extinction curve, the 2175 Å extinction bump is widely seen in the Milky Way (e.g., see Valencic et al. 2004) and external galaxies, both near (e.g., see Declair et al. 2019, Wang et al. 2022, Gordon et al. 2024) and far (see Shivaie et al. 2022, Lin et al. 2023, and references therein).

More recently, utilizing the *Near Infrared Spectrograph* (NIRSpec) on board JWST, Witstok et al. (2023) detected the 2175 Å extinction bump in JADES-GS+53.15138-27.81917 (also known as JADES-GS-z6-0), a distant galaxy at redshift $z \approx 6.71$, corresponding to a cosmic age of just 800 million years (Myr) after the Big Bang.

The identification of the carrier of the 2175 Å extinction bump is relevant for interpreting the UV emission from dis-

tant galaxies observed with JWST. Immediately after its detection nearly 60 years ago (Stecher 1965), the 2175 Å bump was attributed to small graphite grains (Stecher & Donn 1965). If the bump is indeed due to small graphite grains, the detection of the 2175 Å extinction bump at $z \approx 6.71$ indicates that galaxies less than 1 Gyr from the Big Bang were already forming abundant small graphite grains. To interpret JWST observations of high redshift galaxies, it is imperative to place constraints on the nature of the 2175 Å bump carrier. In this regard, JADES-GS-z6-0 provides a valuable opportunity to examine this enigmatic extinction bump. In this work, we aim to quantitatively investigate if small graphite grains can explain the UV extinction bump detected by JWST in JADES-GS-z6-0. This paper is organized as follows. In §2 we model the observed UV extinction bump in terms of small graphite grains. The results and implications are discussed in §3. Our major conclusion is summarized in §4.

2 GRAPHITE AS AN EXPLANATION FOR THE EXTINCTION BUMP

JADES-GS-z6 is located in a portion of an area of the sky known as GOODS-South, which was observed as part of the *JWST Advanced Deep Extragalactic Survey* (JADES; see Eisenstein et al. 2023). JADES-GS-z6 is a low-metallicity, normal star-forming galaxy with a subsolar metallicity of $Z \approx 0.2\text{--}0.3 Z_{\odot}$ and a star formation rate (SFR) of a few

* xjyang@xtu.edu.cn

† lia@missouri.edu

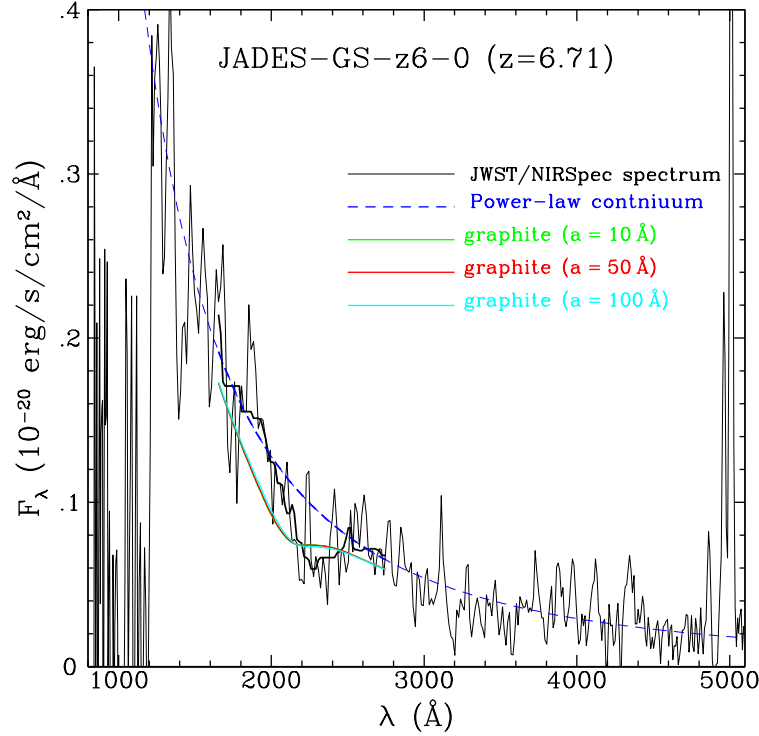


Figure 1. Comparison of the rest-frame UV spectrum of JADES-GS-z6 measured by JWST/NIRSpec (gray solid line) with the dust-attenuated model spectra generated from the power-law continuum (blue dashed line) attenuated by extinction arising from spherical graphite grains of radii of $a = 10 \text{ \AA}$ (green solid line), 50 \AA (red solid line), and 100 \AA (cyan solid line). Note that the green solid line is essentially hidden by the red solid line. The thick black solid line represents a running median and highlights the UV bump region around 2175 \AA . Apparently, graphite dust produces too broad a UV bump to agree with the JWST/NIRSpec spectrum. The model UV bump also fails to peak at the same wavelength as observed by JWST/NIRSpec.

solar masses per year (Witstok et al. 2023). The Balmer decrement as measured from the $H\alpha/H\beta$ line ratio indicates a nebular extinction of $E(B - V) \approx 0.25 \pm 0.07 \text{ mag}$ (see Witstok et al. 2023), demonstrating that this galaxy suffers significant dust obscuration. As illustrated in Figure 1, the rest-frame UV spectrum obtained by JWST exhibits a pronounced dip at wavelength $\lambda_0 \sim 2263^{+20}_{-24} \text{ \AA}$, with a width (measured in wavelength) of $\Delta\lambda \sim 250 \text{ \AA}$ which corresponds to width (measured in inverse wavelength) $\gamma \sim 0.49 \mu\text{m}^{-1}$.¹ This dip resembles the interstellar UV extinction bump but shifting the nominal peak wavelength of 2175 \AA to a somewhat longer wavelength. Its width is considerably narrower than the mean width of $\Delta\lambda \sim 473 \text{ \AA}$ (or $\gamma \sim 1 \mu\text{m}^{-1}$) of the Milky Way ISM (Valencic et al. 2004). In the following, we will follow the custom and refer this dip as the “ 2175 \AA ” extinction bump despite it peaks at 2263 \AA .

Let F_λ^{intr} be the intrinsic, “extinction-free” flux emitted by JADES-GS-z6 at wavelength λ that would be “detected” by JWST,² and F_λ^{mod} be the dust-attenuated “model” flux expected to be observed by JWST. F_λ^{mod} and F_λ^{intr} are re-

lated through

$$F_\lambda^{\text{mod}} = F_\lambda^{\text{intr}} \exp(-\tau_\lambda) \quad , \quad (1)$$

where τ_λ is the optical depth at wavelength λ arising from the dust along the line of sight toward the region in JADES-GS-z6 observed by JWST.³ Assuming a single dust species of a single size a and a column density of N_d , we derive the optical depth from

$$\tau_\lambda = N_d \times C_{\text{ext}}(a, \lambda) \quad , \quad (2)$$

where $C_{\text{ext}}(a, \lambda)$ is the extinction cross section of the dust of size a at wavelength λ . Let’s consider spherical graphite dust of radius a . Let $[C/H]_{\text{gra}}$ be the amount of carbon (C) relative to hydrogen (H) locked up in graphite dust. The dust column density (N_d) relates to the hydrogen column

³ We note that, strictly speaking, τ_λ includes also foreground dust in the Milky Way galaxy along the line of sight toward JADES-GS-z6. However, the foreground reddening between g and r bands derived from the Galactic extinction map of Green et al. (2015) is only $E(g - r) \approx 0.025 \text{ mag}$, corresponding to a visual extinction of $A_V \approx 0.057 \text{ mag}$. Based on the typical wavelength dependence of the Galactic UV, optical and near infrared extinction (see Cardelli et al. 1989, Gordon et al. 2009, Fitzpatrick et al. 2019, Gordon et al. 2021, Declair et al. 2022, Gordon et al. 2023, Wang & Chen 2024), this translates into a negligible amount of foreground extinction in the NIRSpec wavelength range.

¹ Witstok et al. (2023) determined these parameters by fitting the dip with a Drude profile of width $\Delta\lambda$ centered at λ_0 .

² Strictly speaking, this is not dust-free, instead, it is a *continuum* emission which suffers continuum dust attenuation but just free of *extra* extinction at the bump. For more details see §3.

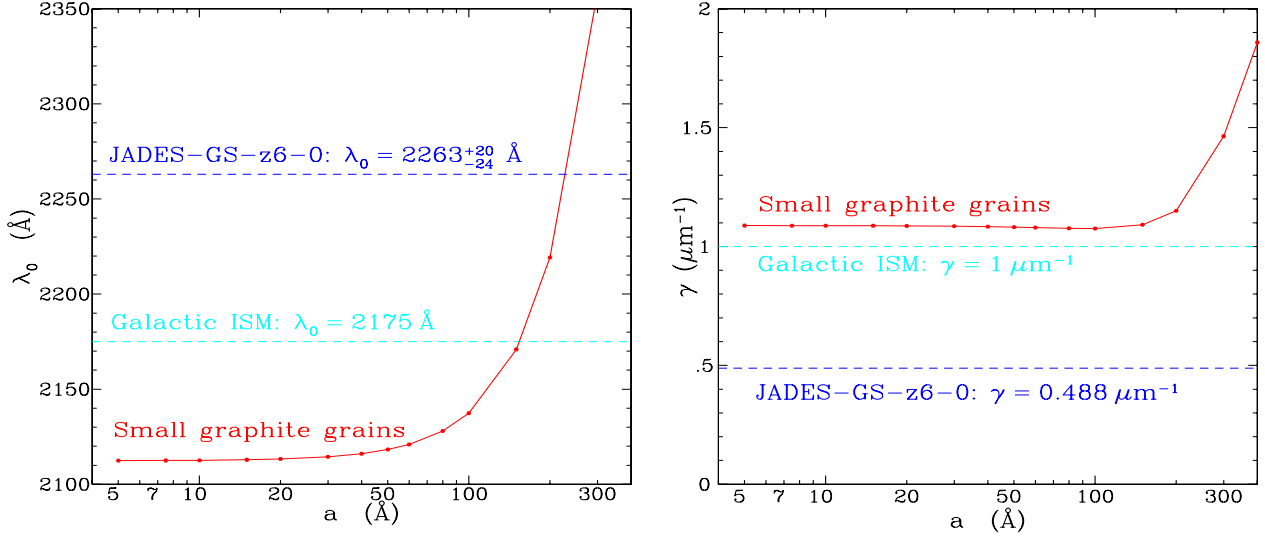


Figure 2. Central wavelength (λ_0 ; left panel) and width (γ ; right panel) of the UV bump calculated from small graphite spheres of radii (a) ranging from a few angstroms to a few tens of nanometers. Horizontal lines plot the central wavelengths and widths of the Galactic average extinction bump and that of the high- z galaxy JADES-GS-z6 at an epoch of the cosmic dawn. It is apparent that the UV bumps resulting from small graphite grains are far too broad and peak at wavelengths that are too short to be consistent with that observed in JADES-GS-z6.

density (N_H) through

$$N_d = N_H \times \left[\frac{C}{H} \right]_{\text{gra}} \times \frac{12 m_H}{(4\pi/3) a^3 \rho_{\text{gra}}} , \quad (3)$$

where m_H is the mass of a hydrogen atom, and $\rho_{\text{gra}} \approx 2.22 \text{ g cm}^{-3}$ is the mass density of graphite. Therefore, the optical depth τ_λ becomes

$$\tau_\lambda = N_H \times \left[\frac{C}{H} \right]_{\text{gra}} \times \frac{C_{\text{ext}}(a, \lambda)}{N_C} , \quad (4)$$

where N_C is the number of C atoms contained in a graphite dust grain of radius a

$$N_C = \frac{(4\pi/3) a^3 \rho_{\text{gra}}}{12 m_H} . \quad (5)$$

To best reproduce F_λ^{obs} , the flux observed by JWST, we require to minimize

$$\chi^2 = \sum_{i=1}^{N_{\text{data}}} \omega'^2 \left\{ \frac{\ln F_\lambda^{\text{obs}} - \ln F_\lambda^{\text{mod}}}{\sigma'_{\text{obs}, \lambda}} \right\}^2 , \quad (6)$$

where $N_{\text{data}} = 33$ is the number of the JWST/NIRSpec data points of JADES-GS-z6 in the wavelength range of 1993.1–2488.7 Å where the observed UV extinction bump peaks, ω' is the weight we introduce here to enhance the fit to the bump, and $\sigma'_{\text{obs}, \lambda}$ is the reduced observational uncertainty:

$$\sigma'_{\text{obs}, \lambda} \equiv \sigma_{\text{obs}, \lambda} / F_\lambda^{\text{obs}} , \quad (7)$$

where $\sigma_{\text{obs}, \lambda}$ is the observational uncertainty. We adopt the following weight

$$\omega' = \begin{cases} 0, & |\lambda - \lambda_0| > 2\Delta\lambda, \\ 1, & \Delta\lambda < |\lambda - \lambda_0| < 2\Delta\lambda, \\ 2, & \Delta\lambda/2 < |\lambda - \lambda_0| < \Delta\lambda, \\ 4, & |\lambda - \lambda_0| < \Delta\lambda/2, \end{cases} \quad (8)$$

where λ_0 and $\Delta\lambda$ are the peak wavelength and full width half maximum (FWHM) of the “2175 Å” UV extinction bump. While rather arbitrarily, we design such a weight to “force” the model spectrum to fit the bump, with *increasing* emphasis paid to the data in the wavelength range *closer* to the bump peak.

By defining $\eta_{\text{gra}} \equiv N_H \times [C/H]_{\text{gra}}$, we achieve the best-fit under the condition of

$$\partial\chi^2 / \partial\eta_{\text{gra}} = 0 , \quad (9)$$

and from eq. 9 we derive

$$\eta_{\text{gra}} = \sum_{j=1}^{N_{\text{data}}} \left\{ \frac{(\ln F_\lambda^{\text{intr}} - \ln F_\lambda^{\text{obs}}) \times (C_{\text{ext}}/N_C)}{\sigma'_{\text{obs}, \lambda}{}^2} \right\} \times \left\{ \sum_{j=1}^{N_{\text{data}}} \left[\frac{C_{\text{ext}}/N_C}{\sigma'_{\text{obs}, \lambda}} \right]^2 \right\}^{-1} . \quad (10)$$

We use Mie theory to calculate the UV extinction cross sections of graphite grains (Bohren & Huffman 1983). We adopt the dielectric functions of graphite of Draine & Lee (1984) and Li & Draine (2001). Graphite is a highly anisotropic material. Its dielectric function depends on the orientation of the electric field relative to the “crystal axis”, or “c-axis” normal to the “basal plane”. For electric fields \vec{E} parallel to the c-axis, the dielectric function is ε_{\parallel} ; for \vec{E} perpendicular to the c-axis, the dielectric function is ε_{\perp} . We take the “1/3–2/3” approximation in which the optical properties of graphite are represented by a mixture of “isotropic” spheres, with 1/3 of which have dielectric functions $\varepsilon = \varepsilon_{\parallel}$; and 2/3 of which have $\varepsilon = \varepsilon_{\perp}$ (see Draine & Malhotra 1993).

We calculate the extinction cross sections of graphite in the wavelength range of 0.1–0.5 μm . We consider a range of graphite sizes, from $a = 5 \text{ \AA}$ up to $a = 0.3 \mu\text{m}$. Both wavelengths and sizes are finely spaced. We present in Figure 1

the best-fit model spectra given by several graphite sizes. For illustrative purposes, we show the model spectra $F_{\lambda}^{\text{mod}}(\lambda)$ created by attenuating the intrinsic spectrum $F_{\lambda}^{\text{intr}}(\lambda)$ with an optical depth τ_{λ} arising from spherical graphite dust grains of radii of $a = 10 \text{ \AA}$, 50 \AA and 100 \AA . Following Wittok et al. (2023), we approximate the intrinsic spectrum by a power-law spectrum which fits the UV continuum observed by JWST/NIRSpec:⁴

$$F_{\lambda}^{\text{intr}}(\lambda) = (0.236 \pm 0.012) \times 10^{-20} \times \left(\frac{\lambda}{1500 \text{ \AA}} \right)^{-2.13} \text{ erg s}^{-1} \text{ cm}^{-2} \quad (11)$$

We find that no matter what sizes are assumed for graphite dust, the model spectra show a bump too broad to reproduce the observed UV bump.

3 DISCUSSION

In the Milky Way, the central wavelength (λ_0) of the 2175 Å extinction bump is essentially invariant, while the bump width ($\Delta\lambda$) shows considerable variation: λ_0 varies by only $\pm 0.46\%$ (2σ) around 2175 Å, in contrast, γ varies by $\pm 12\%$ (2σ) around 473 Å (see Fitzpatrick & Massa 1986, Valencic et al. 2004, Wang et al. 2023). With $\lambda_0 \approx 2263_{-24}^{+20} \text{ \AA}$, the UV bump seen in JADES-GS-z6 peaks at a substantially longer wavelength. JADES-GS-z6 exhibits a much narrower bump ($\Delta\lambda \approx 250 \text{ \AA}$, $\gamma \approx 0.49 \mu\text{m}^{-1}$), even narrower than the narrowest UV bumps of the Milky Way interstellar lines of sight ($\gamma \approx 0.75 \mu\text{m}^{-1}$; see Valencic et al. 2004).

In Figure 2 we plot the central wavelength λ_0 and width γ of the UV bump arising from small graphite spheres as a function of radius a . It clearly demonstrates that small graphite grains (with $a < 230 \text{ \AA}$) produce a UV bump peaking at a wavelength too short to agree with what was seen in JADES-GS-z6. Also, the UV bump caused by small graphite spheres is far too broad to explain that of JADES-GS-z6. Complementary to Figure 1, Figure 2 clearly demonstrates that small graphite spheres are not able to account for the UV bump detected at the cosmic dawn in JADES-GS-z6. We note that for $a \lesssim 100 \text{ \AA}$ the bump central wavelength and width show little variations with grain size. This is not unexpected: for grains in the Rayleigh regime ($2\pi a/\lambda \ll 1$), the extinction profile is essentially independent of grain size (see Bohren & Huffman 1983).

So far, we have focused on spherical grains. Interstellar grains must be nonspherical as indicated by the detection of interstellar polarization. However, for most sightlines, the 2175 Å extinction bump is unpolarized.⁵ The lack of 2175 Å polarization does not necessarily imply that the carriers of the 2175 Å extinction bump must be spherical; instead, they could be nonspherical but not aligned. However, even if they are nonspherical, it is still unlikely for them to be capable of explaining the UV bump observed in JADES-GS-z6. As

demonstrated in Figure 11 of Draine & Malhotra (1993), the bump increasingly broadens and the bump peak shifts to shorter wavelengths as prolate grains become more elongated. Compared with the bump of JADES-GS-z6, the UV bump arising from prolate graphite grains is too broad and peaks at wavelengths that are too short. Therefore, prolate graphite grains are not able to account for the bump of JADES-GS-z6. For oblate graphite grains, the bump width decreases and the bump peak shifts to longer wavelength as the oblateness increases. Nevertheless, to produce a bump as narrow as that of JADES-GS-z6 ($\gamma \approx 0.49 \mu\text{m}^{-1}$), one requires extremely flattened oblates (see the middle panel of Figure 11 of Draine & Malhotra [1993]). However, the bump arising from such extremely elongated oblates would peak at wavelengths considerably longer than that of JADES-GS-z6 ($\lambda_0^{-1} \approx 4.42 \mu\text{m}^{-1}$; see the upper panel of Figure 11 of Draine & Malhotra [1993]). Therefore, we conclude that spheroidal graphite grains are not able to explain the UV bump seen in JADES-GS-z6.

As described in §2, the intrinsic spectrum ($F_{\lambda}^{\text{intr}}$) of JADES-GS-z6 is approximated by the power-law fit to the UV continuum. The underlying assumption for this approximation is that there is little extinction in the wavelength range outside of the UV bump. This is not true: both in the Milky Way and in nearby galaxies (e.g., the Large and Small Magellanic Clouds, and M31), the extinction steeply increases with inverse wavelength (λ^{-1}) toward the far-UV. Therefore, the continuum beyond $\lambda < 2000 \text{ \AA}$ is not really the true stellar continuum emission, instead, it has also been affected by dust extinction. As a matter of fact, the emission of JADES-GS-z6 at all wavelengths is affected by dust attenuation, although the attenuation is less severe at longer wavelengths. In the wavelength range of the bump, there is also continuum attenuation. Nevertheless, in this work as we are mostly interested in the UV extinction bump, it is therefore reasonable to ignore the continuum extinction outside of the wavelength range of the bump. If we are to derive the extinction curve from the optical to the far-UV, the power-law fit to the UV continuum is not a valid representation of the stellar continuum.

Finally, we note that so far we have treated the UV bump seen in JADES-GS-z6 as an extinction feature. However, in extended objects such as external galaxies, where individual stars cannot be resolved, one cannot measure extinction but attenuation. While extinction represents the loss of starlight out of the observer’s line of sight as a result of both absorption and scattering, attenuation is a combination of absorption, scattering out of the line of sight as well as scattering into the line of sight. Therefore, the complex geometry between stars and dust has to be taken into account when one tries to constrain the nature of the carrier of the attenuation bump. This requires complex radiative transfer simulations (e.g., see Seon & Draine 2016, Salim & Narayanan 2020). As radiative transfer would flatten the bump (e.g., see Seon & Draine 2016),⁶ the UV attenuation

⁴ As mentioned earlier, this power-law UV “continuum” spectrum is not really the true, dust-free emission from JADES-GS-z6. It merely approximates the intrinsic continuum emission of JADES-GS-z6 subjected to continuum dust attenuation.

⁵ To date, only two Galactic lines of sight toward HD 147933 and HD 197770 have a weak 2175 Å polarization feature detected (Clayton et al. 1992; Anderson et al. 1996).

⁶ Indeed, the attenuation curves derived for starburst galaxies lack the UV bump at 2175 Å (Calzetti et al. 1994). This is commonly explained in terms of radiative transfer effects (e.g., see Gordon et al. 1997, Witt & Gordon 2000, Fischera et al. 2003, Seon & Draine 2016).

bump seen in JADES-GS-z6 would imply an even *narrower* “intrinsic” extinction bump, too narrow to be accounted for by graphite grains.

We also note that, although small graphite grains are unlikely the carrier candidate material responsible for the UV extinction seen in JADES-GS-z6, graphite is expected to be present in this galaxy (Yang & Li 2023). If star formation began when the Universe was about 400 Myr old, at the epoch of JADES-GS-z6-0 (about 800 Myr old), even the oldest stars were only 400 Myr old. Therefore, there was not enough time for low- to intermediate-mass stars ($\sim 0.5\text{--}8 M_{\odot}$) to evolve sufficiently to the dust-producing “asymptotic giant branch” (AGB) phase. In the Milky Way, AGB stars dominate the production of stardust and typically, it takes them one billion years (Gyr) to evolve. As only massive stars (with a stellar mass of at least $8 M_{\odot}$) would have been able to evolve in such a short time scale (as that available for JADES-GS-z6-0), it is often suggested that supernovae were responsible for the dust in the first billion years of cosmic time (e.g., see Todini & Ferrara 2001, Nozawa et al. 2003, Sugerman et al. 2006, Bianchi & Schneider 2007, Sarangi & Cherchneff 2015, Yang & Li 2023). Supernovae in the Milky Way certainly make graphite as supernova-condensed graphite grains have been identified in primitive meteorites (Nittler & Ciesla 2016). As supernovae are likely the only dust source at the cosmic dawn, it is reasonable to expect graphite grains to be present in the ISM of JADES-GS-z6-0. Perhaps these graphite grains in JADES-GS-z6-0 are like those found in meteorites that are so large ($1\text{--}20 \mu\text{m}$ in diameter) that they could not produce any absorption band around $2,175 \text{ \AA}$. Therefore, species other than graphite, e.g., polycyclic aromatic hydrocarbon molecules (Lin et al. 2025), carbon buckyonions (Li et al. 2008), and even T-carbon (Sheng et al. 2011, Ma et al. 2020), must be responsible for the 2175 \AA bump.

4 SUMMARY

We have examined the UV extinction bump detected by JWST/NIRSpec at an epoch of cosmic dawn in JADES-GS-z6-0, a highly-redshifted galaxy at $z \approx 6.71$. It is found that small graphite grains produce an UV extinction bump that is too broad and peaks at wavelengths that are too short to be consistent with that seen in JADES-GS-z6-0. Species other than graphite (e.g., polycyclic aromatic hydrocarbon molecules) should be explored as possible candidate carriers for the UV extinction bump.

ACKNOWLEDGEMENTS

We thank the anonymous referee for his/her valuable comments and suggestions. We thank J. Witstok for providing us with the JWST/NIRSpec data of JADES-GS-z6. We thank B.T. Draine, Q. Lin, C.E. Mentzer, Q. Wang, J. Witstok and B. Yang for stimulating discussions. QL and XJY are supported in part by NSFC 12122302 and 11873041.

DATA AVAILABILITY

The data underlying this article will be shared on reasonable request to the corresponding authors.

REFERENCES

- Anderson, C.M., Weitenbeck, A.J., Code, A.D., et al. 1996, *AJ*, 112, 2726
- Bianchi, S. & Schneider, R. 2007, *MNRAS*, 378, 973
- Bohren, C.F., & Huffman, D.R. 1983, *Absorption and Scattering of Light by Small Particles* (New York: Wiley)
- Calzetti, D., Kinney, A.L., & Storchi-Bergmann, T. 1994, *ApJ*, 429, 582
- Cardelli, J.A., Clayton, G.C., & Mathis, J.S. 1989, *ApJ*, 345, 245
- Cecchi-Pestellini, C., Mallocci, G., Mulas, G., Joblin, C., & Williams, D.A. 2008, *A&A*, 486, L25
- Clayton, G.C., Anderson, C.M., Magalhaes, A.M., et al. 1992, *ApJL*, 385, L53
- Decleir, M., De Looze, I., Boquien, M., et al. 2019, *MNRAS*, 486, 743
- Decleir, M., Gordon, K. D., Andrews, J. E., et al. 2022, *ApJ*, 930, 15
- Draine, B.T., & Lee, H.M. 1984, *ApJ*, 285, 89
- Draine, B.T. & Malhotra, S. 1993, *ApJ*, 414, 632
- Eisenstein, D. J., Willott, C., Alberts, S., et al. 2023, *ApJ*, submitted (arXiv:2306.02465)
- Fischera, J., Dopita, M. A., & Sutherland, R. S. 2003, *ApJL*, 599, L21
- Fitzpatrick, E. L., & Massa, D. 1986, *ApJ*, 307, 286
- Fitzpatrick, E. L., Massa, D., Gordon, K. D., et al. 2019, *ApJ*, 886, 108
- Gordon, K.D., Calzetti, D., & Witt, A.N. 1997, *ApJ*, 487, 625
- Gordon, K. D., Clayton, G. C., Misselt, K. A., et al. 2003, *ApJ*, 594, 279
- Gordon, K. D., Cartledge, S., & Clayton, G. C. 2009, *ApJ*, 705, 1320
- Gordon, K. D., Misselt, K. A., Bouwman, J., et al. 2021, *ApJ*, 916, 33
- Gordon, K. D., Clayton, G. C., Decleir, M., et al. 2023, *ApJ*, 950, 86
- Gordon, K. D., Fitzpatrick, E. L., Massa, D., et al. 2024, *ApJ*, 970, 51
- Green, G. M., Schlafly, E. F., Finkbeiner, D. P., et al. 2015, *ApJ*, 810, 25
- Li, A., & Draine, B. T. 2001, *ApJ*, 554, 778
- Li, A., Chen, J.H., Li, M.P., Shi, Q.J., & Wang, Y.J. 2008, *MNRAS*, 390, L39
- Lin, Q., Yang, X.J., & Li, A. 2023, *MNRAS*, 525, 2380
- Lin, Q., Yang, X.J., Li, A., & Witstok, J. 2025, *A&A*, 694, A84
- Ma, X.Y., Zhu, Y.Y., Yan, Q.B., You, J.Y., & Su, G. 2020, *MNRAS*, 497, 2190
- Nozawa, T., Kozasa, T., Umeda, H., Maeda, K., & Nomoto, K. 2003, *ApJ*, 598, 785
- Salim, S., & Narayanan, D. 2020, *ARA&A*, 58, 529
- Sarangi, A., & Cherchneff, I. 2015, *A&A*, 575, A95
- Seon, K.-I., & Draine, B. T. 2016, *ApJ*, 833, 201
- Shivaei, I., Boogaard, L., Díaz-Santos, T., et al. 2022, *MNRAS*, 514, 1886
- Stecher, T. P. 1965, *ApJ*, 142, 1683
- Stecher, T. P. & Donn, B. 1965, *ApJ*, 142, 1681
- Sugerman, B. E. K., Ercolano, B., Barlow, M. J., et al. 2006, *Science*, 313, 196
- Todini, P., & Ferrara, A. 2001, *MNRAS*, 325, 726
- Valencic, L. A., Clayton, G. C., & Gordon, K. D. 2004, *ApJ*, 616, 912
- Wang, Q., Yang, X.J., & Li, A. 2023, *MNRAS*, 525, 983
- Wang, S., & Chen, X. 2024, *ApJL*, 964, L3
- Wang, Y., Gao, J., & Ren, Y. 2022, *ApJS*, 259, 12
- Witstok, J., Shivaei, I., Smit, R., et al. 2023, *Nature*, 621, 267
- Witt, A.N., & Gordon K.D. 1996, *ApJ*, 463, 681
- Yang, X.J., & Li, A. 2023, *Nature*, 621, 260